A Discrete RET Model for Millimeter-Wave Propagation Through Vegetation

Nuno R. Leonor, *Student Member, IEEE*, Rafael F. S. Caldeirinha, *Senior Member, IEEE*, Telmo R. Fernandes, *Senior Member, IEEE*, Jürgen Richter, and Miqdad Al-Nuaimi

***Abstract*— A modified discrete radiative energy transfer (dRET) model has been developed envisaging to overcome some of the limitations found in the original dRET formulation, namely in terms of angular resolution, oblique and nonuniform incidence, and antenna patterns. In addition, the discretized squared nature of the dRET model can lead to some amount of staircase error. Hence, this paper also proposes an input parameter scaling model, enabling the characterization of tree cells with reduced size. The performance of the modified dRET model is assessed not only against the current ITU-R P.833-8 recommendation for propagation in vegetation but also against directional spectra measurements conducted in an outdoor inhomogeneous forest at 20 and 62.4 GHz.**

***Index Terms*— Millimeter wave propagation, modeling, scattering, vegetation.**

I. Introduction

HISTORICALLY, two distinct theories have been developed to deal with multiple scattering phenomena [1]: the analytical [2]–[4] and the transport theories [6]–[8]. The analytical theory, based on Maxwell's differential equations, completely describes the physical electromagnetic phenomena taking place in any propagation medium. To obtain this mathematically rigorous description of the scattering phenomena, a complete knowledge of the medium is required. In the particular case of radiowave propagation through vegetation media, such deterministic models rapidly become impractical [5], [6], since the detailed positions and orientations for every element of the forest, including tree trunks, branches, leaves, and so on, are difficult to obtain in a real environment.

Manuscript received August 2, 2016; revised December 19, 2017; accepted February 12, 2018. Date of publication February 15, 2018; date of current version April 5, 2018. This work was supported in part by the University of South Wales, Pontypridd CF37 1DL, U.K., in part by the Instituto de Telecomunicações, Portugal, through IT/LA under Grant UID/EEA/50008, and in part by the Portuguese Government, Portuguese Foundation for Science and Technology through the POPH/FSE Fund. (Corresponding author: Rafael F. S. Caldeirinha.)

N. R. Leonor is with the Instituto de Telecomunicações, 2411-901 Leiria, Portugal, and also with the Departamento de Teoria do Sinal e Comunicacións, University of Vigo, 36200 Vigo, Spain.

R. F. S. Caldeirinha and T. R. Fernandes are with the Instituto de Telecomunicações, 2411-901 Leiria, Portugal, also with the Polytechnic Institute of Leiria, School of Technology and Management, 2411-901 Leiria, Portugal, and also with the Wireless and Optoelectronics Research and Innovation Centre, University of South Wales, Pontypridd CF37 1DL, U.K. (e-mail: rafael.caldeirinha@ipleiria.pt).

J. Richter and M. Al-Nuaimi are with the Wireless and Optoelectronics Research and Innovation Centre, University of South Wales, Pontypridd CF37 1DL, U.K.

Color versions of one or more of the figures in this paper are available online at http://ieeexplore.ieee.org.

Digital Object Identifier 10.1109/TAP.2018.2806393

Instead of starting from elementary wave equations, the transport theory deals directly with the transport of the energy throughout a medium containing randomly distributed particles. Although this theory is heuristic and lacks the mathematical rigor of the analytical theory, the radiative energy transfer (RET) theory is a widely used method to model the wave propagation through random scattering media [1], predicting signal attenuation, scattering, and (de)polarization due to the presence of vegetation in the radio path [6]–[12]. Notwithstanding, despite the recent advances in electromagnetic scattering by discrete random media [13], [14], the inhomogeneity intrinsic to vegetation scenarios justifies the need for a model that can accommodate such challenging propagation characteristics.

The discrete RET (dRET) approach [15] consists of a technique intended to deal with the isolated volumes of vegetation, consequently overcoming some of the limitations found in the original RET formulation presented in [6] and [8]. The dRET divides the medium into several nonoverlapping vegetation cells, each with specific propagation characteristics. The original dRET approach was exclusively aimed at overcoming the RET infinite space limitation, allowing its application to isolated vegetation structures. However, in its original form [15], this modeling approach still presents limitations. To this extent, the limitations of the original dRET model will be investigated throughout this paper and enhancements sought to overcome such limitations will be proposed.

This paper is organized as follows. Section II outlines the original dRET formulation as presented in [15]. In Section III, the limitations of the dRET model are systematically investigated and a modified dRET model is proposed. The extraction methods of the required input propagation parameters are discussed in Section IV, including a parameter scaling model which enables the characterization of large volumes of vegetation with various smaller cells, reducing the discretization staircase error. Section V presents a performance analysis of the modified dRET model directional spectra predictions for an outdoor inhomogeneous forest, not only against the current ITU-R P.833-8 recommendation for propagation in vegetation but also against outdoor measurements conducted at 20 and 62.4 GHz. Finally, Section VI draws conclusions and points out directions for further work.

II. Original dRET Formulation

The original dRET approach consists of dividing the vegetation volume into several nonoverlapping cells [15], as depicted in Fig. 1, allowing the modeling of isolated vegetation struc-

tures. The vegetation cells are considered to be identical in size, i.e., constant Δs, and are identified by their Cartesian coordinates (k, l, m).

The total signal intensity in each cell is decomposed into the reduced ($I_{\rm ri}$) and diffuse (I_d) intensities, corresponding to the coherent and incoherent components, respectively. These signal intensities are evaluated using an iterative process that starts at the air–vegetation interface, where $I_{\rm ri}^{\rm IN} = I_o(\gamma_0)$ is known, and proceeds across the entire structure several times to evaluate all the interactions between adjacent cells, until a steady-state criteria is reached [15]. While both the input and output coherent intensities exhibit the same definite direction, each input diffuse intensity component $I_d^{\rm IN}$ generates several output components due to the scattering process. The relations between input and output intensities are derived from the original RET formulation [8], [9] and were simplified using piecewise linear approximations. The piecewise linear approximations for $I_{\rm ri}$ and I_d are, respectively, expressed by

$$I_{\rm ri}^{\rm OUT}(\gamma_0) = I_{\rm ri}^{\rm IN}(\gamma_0) - k_e I_{\rm ri}^{\rm IN}(\gamma_0)\Delta s \tag{1}$$

$$I_d^{\rm OUT}(\gamma) = I_d^{\rm IN}(\gamma) + \left[-k_e I_d^{\rm IN}(\gamma)\right]\Delta s + \left[k_s \sum_{\gamma'=1}^{26} P(\gamma, \gamma') I_d^{\rm IN}(\gamma') + k_s P(\gamma, \gamma_0) I_{\rm ri}^{\rm IN}(\gamma_0)\right]\Delta s \tag{2}$$

where $I_{\rm ri}^{\rm IN}$ and $I_{\rm ri}^{\rm OUT}$ are the input and output reduced intensities, $I_d^{\rm IN}$ and $I_d^{\rm OUT}$ are the input and output diffuse intensities, and k_e and k_s are the extinction and the scattering coefficients. In (2), the thermal radiation of the absorbing volume is neglected, since it is assumed that the particles' temperature is not high enough to make the emission component of the radiation field comparable to the scattered one. To manage the scattering profile of the dRET vegetation cells, a so-called phase function was used, which is modeled as a Gaussian shaped forward lobe, superimposed to an isotropic level representing the backscattering region. The phase function, originally proposed in [17], is described as

$$P(\psi) = \alpha \left(\frac{2}{\beta}\right)^2 e^{-\left(\frac{\psi}{\beta}\right)^2} + (1-\alpha) \tag{3}$$

where α is the ratio between the forward lobe power and the total power of the phase function, β represents the half-power beamwidth (HPBW) of the forward lobe and ψ is the angular difference between the incident ($\hat{s}$) and scattering ($\hat{s}'$) directions. Since inside the dRET cubic cell, the vegetation medium is assumed to be homogeneous, the scattering phenomena will not be dependent on the azimuth and elevation. Hence, ψ is not expressed in terms of azimuth and elevation.

In a cubic discrete structure like the one presented in Fig.1, each element cell is surrounded by 26 direct neighbors, thus explaining the sum over the 26 discrete directions [15] in (2). Hence, the discrete phase function $P(\psi)$ is exclusively defined at those 26 discrete directions. From these discrete directions, the smallest nonzero angular direction is 35°. Consequently, if (3) is to be used all the discrete directions except one would

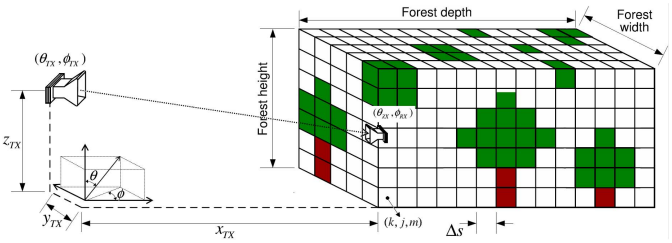

Fig. 1. 3-D dRET forest geometry diagram.

lie outside of the phase function main lobe. To overcome this limitation, a three-step discrete phase function was proposed in [15]. The three levels of this phase function correspond to: 1) the discrete forward scattering direction ($\phi = 0°$); 2) the so-called "directive scattering range" ($0° < \phi \leq 45°$); and 3) the isotropic scattering angular range representing the remaining directions. The step levels from this discrete phase function were defined in [15] using the following three functions:

$$g(\delta\gamma) = \begin{cases} (\alpha - \beta\alpha)D & \delta\gamma = 0 \\ [(1-\alpha) + \beta\alpha]D & 0 < \delta\gamma < \delta\gamma_1 \\ (1-\alpha)D & \delta\gamma_1 \leq \delta\gamma \end{cases} \tag{4}$$

where $\delta\gamma$ represents the discrete angular directions and D is a normalization constant required to fulfill the power conservation criteria. The $\delta\gamma_1$ parameter, which is the maximum discrete direction lying in the directional scattering range, is determined by n_d. This parameter represents the number of discrete angular directions assigned to the directional scattering range.

III. Extended dRET Propagation Model

The enhanced dRET model [16] is sought to overcome some of the limitations from the original dRET model [15]. The formulation of the modified dRET model is based on the forest geometry presented in Fig. 1. The transmitter (TX) antenna is considered to be placed outside the vegetation medium, whereas the receiver (RX) antenna is limited to the geometric centers of the vegetation cells $(k, l, m)_{\rm RX}$ forming the discrete structure.

A. Enhanced Angular Resolution

The original dRET may be regarded as a node-based algorithm where cells are reduced to nodes exhibiting specific scattering properties. The specific signal intensities are only calculated on a cell center basis, limiting the possible signal angular directions at each node to 26 discrete directions. In Fig. 2(a), it is shown that the minimum nonzero angle between the cell centers is 45°, which explains the relatively low angular resolution exhibited by the original dRET results.

To increase the angular resolution of the extended dRET model, an empirical averaging method based on the path length traveled by each ray in the corresponding neighbor cell was developed. Inspired by similar methods proposed in [18] and [19], this is initially for a 2-D situation. As depicted in Fig. 2(b), the referred averaging method distinguishes three different angular regions: Region 1 ($0 \leq \phi \leq 18.43°$); Region 2 ($18.43° < \phi < 45°$); and Region 3 ($\phi = 45°$). Assuming this three-cell geometry, the signal intensities entering cell 1 are

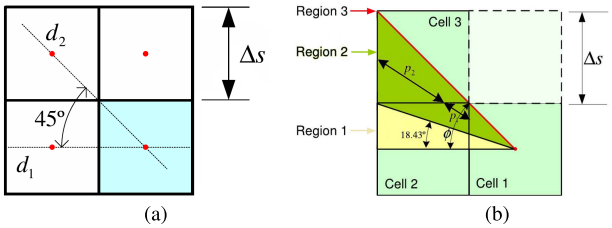

Fig. 2. Schematic of the 2-D dRET cell interaction. (b) Schematic of the averaging method allowing to enhance the dRET angular resolution.

calculated differently depending on their directions and the cell where they were originated. The intensity entering cell 1 through the angular region 1 is simply the intensity flowing out of cell 2 on the selected incoming angles. The angular region 2 is called the averaging region, since the intensity received in this region is considered to be an average of the intensities flowing out of cells 2 and 3. This average is weighted by the normalized paths traveled by each intensity in the corresponding cell. The paths depicted in Fig. 2(b) allow the calculation of the relative weights of the intensity components p_1^n and p_2^n, which are subsequently used in

$$I_{\text{cell1}}^{\text{IN}}(\phi) = I_{\text{cell2}}^{\text{OUT}}(\phi)p_1^n + I_{\text{cell3}}^{\text{OUT}}(\phi)p_2^n \tag{5}$$

to calculate the total intensity originated from region 2. When angles within region 2 are considered, ϕ values close to 18.43° yield to a small p_2 and hence the influence of $I_{\text{cell3}}^{\text{OUT}}$ on $I_{\text{cell1}}^{\text{IN}}$ is minimized, whereas for higher values of ϕ, the influence of cell 3 also increases. At $\phi \approx 45°$, p_1^n is almost 0 and the influence from cell 2 vanishes. At $\phi = 45°$ or region 3, only the energy emanating from cell 3 is considered. This procedure is consistently applied throughout the remaining angular range between 45° and 360°. The values of the weighting functions p_1^n and p_2^n are calculated for the angular region 2, i.e., $18.43° < \phi < 45°$, according to

$$\begin{cases} p_1(\phi) = \dfrac{\Delta s(1-\tan\phi)}{2\sin\phi} \\ p_2(\phi) = \dfrac{\Delta s(-1+3\tan\phi)}{2\sin\phi} \end{cases} \tag{6}$$

and subsequently normalized using

$$p_i^n(\phi) = \frac{p_i(\phi)}{p_1(\phi)+p_2(\phi)}. \tag{7}$$

B. Solving I_{ri} and I_d Equations

As previously mentioned, the original dRET formulation [15] used a piecewise linear approximation to obtain the discrete RET equations (1) and (2). Although this approach is valid when relatively small cell sizes are used, it has caused difficulties in the dRET convergence for cells larger than 1.5 m. The trees generally found in the forests have canopies with 5–20 m of diameter and consequently the original dRET formulation might be unusable for applications where one single tree corresponds to one vegetation cell.

Solutions for a first-order linear differential equation which has the following general form:

$$\frac{d_y}{d_x} + p(x)y = q(x) \tag{8}$$

and its general solution is given by

$$y = \frac{\int u(x)q(x)d_x + C}{u(x)} \tag{9}$$

where,

$$u(x) = e^{\int p(x)d_x} \tag{10}$$

is called the integrating factor, and constant C can be found through the giving of initial conditions. The I_{ri} equation can be assumed to be a first-order linear differential equation exhibiting this general form, considering $q(x) = 0$ and $p(x) = k_e$. Hence, the solutions for the I_{ri} equation can be found based on two initial conditions, depending on whether the first layer of cells or the subsequent layers are being considered. At first cell layer, the initial condition is $I_{\text{ri}}^{\text{IN}}(n = 1) = I_0$, whereas in the subsequent layers, the initial condition is $I_{\text{ri}}^{\text{IN}}(n) = I_{\text{ri}}^{\text{OUT}}(n-1)$, where n stands for the number of the layer being considered. Using these boundary conditions, the following equation can be obtained:

$$I_{\text{ri}}^{\text{OUT}}(\hat{s}_0) = I_{\text{ri}}^{\text{IN}}(\hat{s}_0)e^{-k_e\Delta s} \tag{11}$$

where $\hat{s}_0$ represents the direction of I_{ri}. The I_d equation might be solved using a similar approach, using the boundary conditions relative to the diffused intensity, i.e., $I_d(\hat{s}, n = 0) = 0$ at the first layer; and $I_d^{\text{IN}}(\hat{s}, n) = I_d^{\text{OUT}}(\hat{s}, n-1)$ at the subsequent layers. The solution for I_d can be obtained as

$$\begin{aligned} I_d^{\text{OUT}}(\hat{s}) = {} & \frac{k_s S(\hat{s})}{k_e} \\ & + \frac{k_s P(\hat{s}_0, \hat{s}) I_{\text{ri}}^{\text{IN}}}{k_e} \\ & - \frac{\left[k_s S(\hat{s}) + k_s P(\hat{s}_0, \hat{s}) I_{\text{ri}}^{\text{IN}}\right] e^{-k_e\Delta s}}{k_e} \\ & - I_d^{\text{IN}}(\hat{s}) e^{-k_e\Delta s} \end{aligned} \tag{12}$$

where $S(\hat{s})$ is the weighted contribution from the neighbor cells in direction $\hat{s}$, and $\hat{s}_0$ is the direction of I_{ri} given by

$$S(\hat{s}) = \sum_{\hat{s}'} P(\psi) I_d^{\text{IN}}(\hat{s}') \tag{13}$$

where ψ is the angle between $\hat{s}$ and $\hat{s}'$.

Both the piecewise approach and the proposed approach were used to calculate the signal intensity inside a 100 m × 200 m forest divided into 5 m cells. As depicted in Fig. 3(a), the original dRET modeling approach [15] is unable to converge into a stable result, whereas the proposed formulation provided a relatively good convergence at the end of a few iterations, even for 5 m cells. This is confirmed in Fig. 3(b).

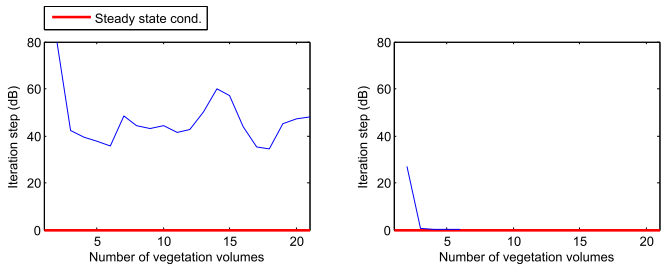

Fig. 3. Convergence evaluation of the enhanced dRET using (a) piecewise linear approximation and (b) complete equations, both considering $\Delta s = 5m$.

C. Receiver Antenna Effect

The RX antenna effect is evident at large vegetation depths where the diffuse signal is dominant. On one hand, as the antenna HPBW increases, the amount of diffuse received signal also increases, whereas, on the other hand, antenna characteristics such as secondary lobes might influence the received signal level and the directional spectrum shape. Hence, the modified dRET model will use its enhanced angular resolution to compute the received signal power for an arbitrary shaped RX antenna, which was not possible to perform in the original dRET model, especially whenever narrow HPBW antennas are used. The received signal power level $R_{k,l,m}$ at a specific location within the forest defined by cell coordinates k, l, m, is given by the sum of the incident specific signal intensities, after being conveniently weighted by the antenna radiation pattern. Such a relation is expressed by

$$R_{k,l,m}(\phi,\theta) = \frac{\lambda_0^2}{4\pi}\sum_{\phi}\sum_{\theta} G_{\mathrm{RX}}(\phi-\phi_{\mathrm{RX}},\theta-\theta_{\mathrm{RX}}) \times I_{k,l,m}(\phi,\theta) \qquad (14)$$

where λ_0 is the signal wavelength, $I_{k,l,m}$ is the incoming signal intensity at the cell located at (k, l, m) position, and G_{RX} is the normalized radiation pattern of the RX antenna.

D. Nonuniform Interface Illumination

In realistic outdoor environment, the uniform interface illumination is normally reached by using broad TX antennas or by placing these antennas at a considerable distance from the air–vegetation interface. Consequently, whenever these conditions are not met, both the RET [8] and dRET formulations [15] are not completely accurate, since they assume a uniform air-to-vegetation interface illumination. To improve the dRET model, the modified dRET implementation not only can accommodate different signal intensities in the interface cells but also calculate these intensities based on the TX antenna position and radiation pattern.

A generic scenario used to calculate the interface illumination is depicted in Fig. 4. In this scenario, x_F, y_F, and z_F represent the forest Cartesian coordinate system, whereas x_A, y_A, and z_A belong to a coordinate system centered on the TX antenna. Finally, the ϕ_{TX} and θ_{TX} angles represent the TX antenna pointing azimuth and elevation angles, respectively.

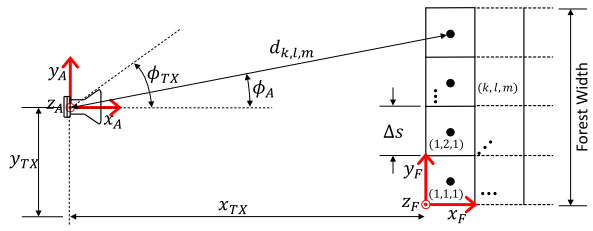

Fig. 4. Geometry for the calculation of the air-to-vegetation interface illumination—Top view ($\theta_{\mathrm{TX}} = 0°$).

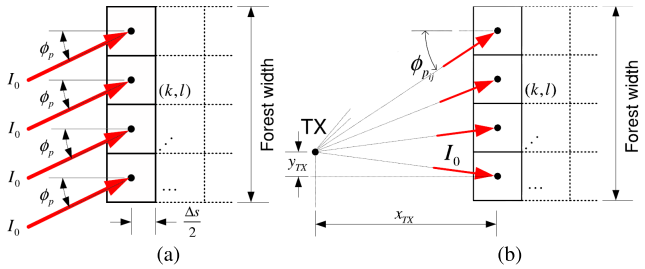

Fig. 5. Impinging rays at the air-to-vegetation interface (a) with oblique incidence (parallel rays) and (b) under point source illumination.

The normalized received power level $R_{k,l,m}$ at the center of each of the air–vegetation interface cells is given by

$$R_{k,l,m}(dB) = 20\log\left(\frac{d_{\min}}{d_{k,l,m}}\right) + G_{\mathrm{TX}}(\theta_A-\theta_{\mathrm{TX}},\phi_A-\phi_{\mathrm{TX}}) \qquad (15)$$

where $d_{\min}$ is the minimum distance between the antenna and the air–vegetation interface, $d_{k,l,m}$ is the distance between the TX and the center of the (k, l, m)th cell, G_{TX} is the normalized radiation pattern of the TX antenna, and (θ_A, ϕ_A) is the angular direction of the departing ray toward the cell under calculation.

E. Oblique Incidence and Point Source Illumination

Whenever a generic propagation through vegetation scenario is to be considered, the incidence angle impinging at the air-to-vegetation interface may differ from normal incidence, and hence, the propagation model should be capable of accommodating an oblique incidence scenario. If the TX antenna is sufficiently distant from the air–vegetation interface, as depicted in Fig. 5(a), the incidence angle of I_0 rays can be considered constant throughout the vegetation structure. However, should the TX be placed at a short range, the incidence angle depends on the vegetation cell under consideration as depicted in Fig. 5(b).

To this extent, the calculation of the coherent intensity emanating from the cells is different depending on whether the incidence is normal or oblique. In the latter, the cell layers are not parallel to the direction of propagation. This is especially important when a point source is considered, and therefore, the angles of propagation depend on the cell under consideration. To calculate the coherent intensity, the original I_{ri} equation must be transformed into

$$I_{\mathrm{ri}}(k,l,m) = I_0 e^{-\sum_{s_i} k_e(k,l,m)\Delta s_i} \qquad (16)$$

where $k_e(k,l,m)$ is the extinction coefficient corresponding to cell (k,l,m), and Δs_i is the path traveled by the coherent signal in the (k,l,m)th cell.

IV. Parameter Extraction Method for Inhomogeneous Vegetation Media

Unlike the RET [8] modeling approach, which assumes a homogeneous medium, the dRET [15] models the vegetation volume as a cellular structure formed by several vegetation blocks exhibiting different propagation characteristics. To this extent, distinct values of the model input parameters must be independently extracted from the different vegetation types forming the medium.

A. Extinction Coefficient k_e Extraction Method

Early work on the extraction extinction coefficient k_e was proposed in [20]. This method is based on two simple measurements. Initially, the TX and RX antennas are placed facing each other at a distance such that the mutual far-field criteria are fulfilled, and the free-space signal level is recorded for normalization purposes. Subsequently, the tree is placed between both TX and RX, and the excess attenuation caused by the tree is recorded. Although this procedure can be easily employed on small plants and thus be suitable for indoor measurements, an alternative method must be employed for outdoor radio paths containing full size trees.

The method proposed here is also based on two measurements performed in front (M_1) and behind (M_3) the tree under consideration, according to Fig. 6. At both M_1 and M_3 measurement positions, the RX antenna is rotated $\pm 45°$ around its vertical axis with $1°$ steps, so the directional profile of the received signal can be obtained. The distances d_1 and d_3, also shown in the figure, are used to calculate the excess free-space loss (FSL), which will be subtracted from the total measured loss. Subsequently, the maximum measured power levels and the relative distances between the TX and the RX measurement positions can be used to calculate k_e according to

$$\frac{M_{3\max}}{M_{1\max}} = e^{-k_e(d_3-d_1)}\left(\frac{d_1}{d_3}\right)^n \tag{17}$$

where n is the decay term of the excess FSL. This term was considered to be $n = 2$, indicating that a single ray model was employed in the FSL calculation. k_e obtained using this method describes the decay of the signal level due to the excess vegetation attenuation, consequently excluding any decay caused by the FSL. Due to this, the value of k_e can be directly used in the dRET coherent component equation to obtain predicted values for the excess attenuation.

The method outlined here will only be exact if the received signal at position M_3 is predominantly due to the coherent signal component. The coherence of the received signal behind the tree may be guaranteed providing that the vegetation depth used during the measurement is small enough. Some experiments reported in [6] and [8] suggest that using a practical vegetation depth corresponding to just one tree yield relatively good results for k_e extraction. Furthermore, the magnitude of incoherent signal received behind the test vegetation block is also influenced by the RX antenna HPBW, which it should be as narrow as possible.

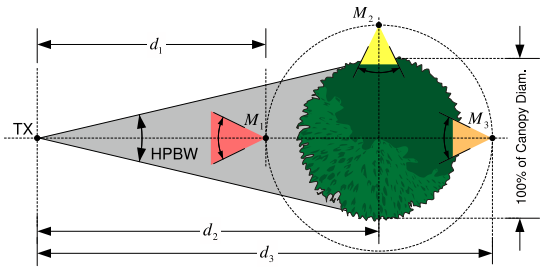

Fig. 6. Measurement geometry for dRET input parameter extraction.

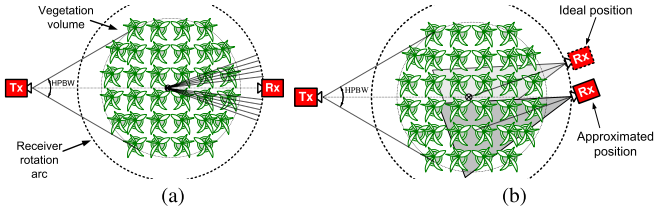

Fig. 7. Reradiation measurement setup. (a) Exact method. (b) Approximated method.

B. Phase Function Estimation

The method adopted to measure the phase function consists of rotating the RX antenna following an arc around the tree [8], [21], recording its normalized scattering profile at each angular position. A diagram of such measurement method is presented in Fig. 7(a). Although the method may be used in an indoor environment, it is not suitable for large vegetation volumes, since it would require moving the RX antenna disturbing the required antenna alignment [22].

To this extent, an approximate measurement method, which minimizes the need for the RX antenna movement, was developed. This method evaluates the phase function beamwidth β based on an RX rotation around its vertical axes rather than a rotation around the vegetation volume. A comparison between the ideal and approximate measurement methods to estimate the β parameter is depicted in Fig. 7(b). As shown in the figure, for small β angles, the common illuminated volume by the RX and the TX antennas is similar for both ideal and approximate measurement positions, and hence, the measured β values are considered to be similar.

The β parameter is subsequently obtained by fitting the normalized Gaussian phase function (3). The fitting is performed by calculating the root mean squared error (RMSE) between the Gaussian phase function and the measured signal profile for a wide range of β parameter values.

Only the β parameter is extracted from the fitting of the Gaussian curve, since the backscatter level is likely to be influenced by the variation of the RX and TX common illumination volume, which decreases as the RX antenna points away from the tree. Therefore, a side scatter measurement is performed at measurement position M_2, to properly evaluate the phase function backscattering level. Similar to the measurements performed for other positions, at M_2, the RX antenna is rotated

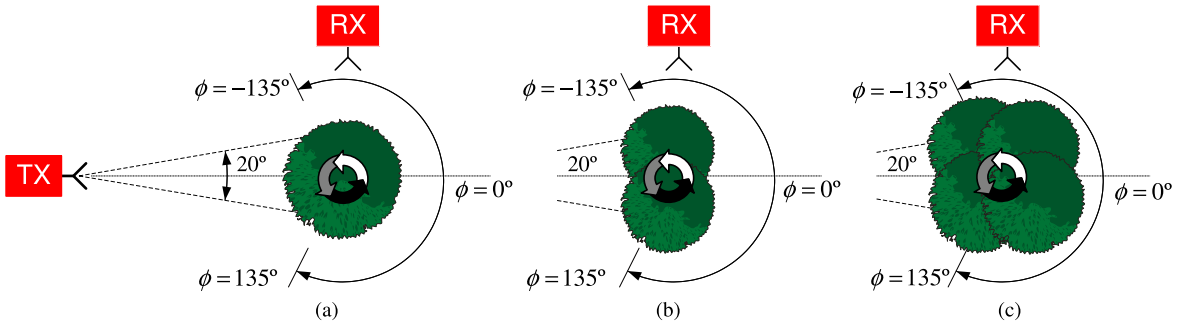

Fig. 8. Indoor reradiation function measurement setup for (a) 1, (b) 2, and (c) 3 plants.

around its vertical axis in a ±45° angular range, recording the received signal with 1° of resolution. The side scattered signal is subsequently calculated by averaging the signal level at each angular position. The normalized signal level obtained from this measurement is used along with the phase function equation (3) to calculate the α parameter value.

C. Scattering Cross Section k_s Extraction Method

To evaluate the vegetation scattering cross section k_s, the geometry adopted to perform the M_2 measurement is modeled using the dRET model as a single dRET vegetation cell, which is uniformly illuminated by the TX antenna. Considering such a scenario, the received signal normalized power level P_{RX} will be given by

$$P_{\mathrm{RX}}(\phi = 90°) = \sum_{\phi_i=-45°}^{45°} G_{\mathrm{RX}}(\phi_i) \frac{I_d(\phi_i + 270°)}{I_0} \tag{18}$$

where I_0 is the maximum intensity at the air-to-vegetation interface (for normalization purposes) and I_d is the diffuse intensity radiated by the vegetation block. The incoherent signal intensity was calculated using the dRET equation to the single vegetation block presented in the propagation scenario. This equation is a simplified version of (12), which ignores any interaction between vegetation cells. This is possible, since the complete tree is modeled using a single dRET cell. The simplified I_d equation is given by

$$I_d(\phi) = \frac{k_s P(\phi) I_{\mathrm{ri}}^{\mathrm{IN}} (1 - e^{-k_e d})}{k_e} \tag{19}$$

where $P(\phi)$ is the phase function given by (3) after an appropriate normalization process to fulfill the power conservation criteria, d is the cell width in meters and $I_{\mathrm{ri}}^{\mathrm{IN}}$ is the input reduced intensity at the single vegetation cell. The input reduced intensity can be determined through

$$I_{\mathrm{ri}}^{\mathrm{IN}} = I_o \tag{20}$$

which represents the signal intensity impinging at the single vegetation cell. Finally, (18)–(20) can be used to optimize k_s such that the received power level $P_{\mathrm{RX}}(\phi = 90°)$ fits the measured side scattered signal obtained from the measurement geometry as shown in Fig. 6.

D. dRET Parameter Scaling

The discretization of the vegetation medium into individual cells eventually produces staircase error, due to the assumption that the signal is invariant throughout the cell volume. This may be minimized by maintaining vegetation cells size as small as possible. On the other hand, as the vegetation cells become smaller, the computational effort to characterize a forest environment is increased, and hence, a tradeoff between model accuracy and computational effort must be achieved.

As far as dRET input parameter extraction is concerned, the method used for k_e and k_s can also be employed for small cells, as they are expressed in a per meter basis. Notwithstanding, the α and β parameters will vary with the vegetation volume size, due to the multiple internal scattering inside the vegetation canopy. Hence, its extraction can be particularly difficult to perform when cells are smaller than the trees to be modeled, since it is impossible to perform reradiation measurements for a portion of a tree.

To this extent, an evaluation of the α and β dependence on the size of the vegetation volume was performed. The experiment used the measurement geometry depicted in Fig. 8(a) to record the reradiation pattern of four *Ficus Benjamina* trees separately, which were named F1, F2, F3, and F4. Tree specimens had a mean canopy diameter of 60 cm and 1.5 m of height, and both F1 and F2 exhibited a relatively sparse leaf structure when compared with F3 and F4. In each measurement, the RX was rotated along an arc around the tree, within an angular range of $\phi = \pm 135°$ with 1° steps. In each RX position, a tree was rotated $\phi_t = 360°$ around its vertical, and 10^6 samples of the received signal level were acquired by a data acquisition card, which were averaged yielding the tree reradiation function. Subsequently, new measurements were conducted to record the reradiation pattern of groups of trees, mimicking trees with different thicknesses. To this extent, tree specimens F2 and F3 were placed side by side, as depicted in Fig. 8(b), and then all the four tree specimens were placed in a square-shaped vegetation volume, as depicted in Fig. 8(c). Measurements were carried out at 20 and 40 GHz using 20 dBi horn antennas at the RX and 10 dBi antennas at the TX. In addition, measurements performed at 62.4 GHz used a 25 dBi horn antenna at the TX and a 10 dBi antenna at the RX end. The distance between the TX antenna and the tree under measurement was selected to ensure that 2/3 of the 60 cm canopy diameter was illuminated by the TX antenna HPBW.

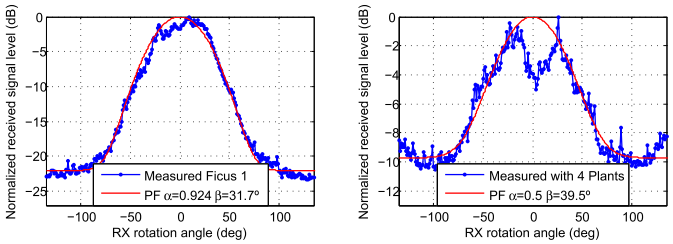

Fig. 9. Measured reradiation functions obtained at 40 GHz for (a) F1 and (b) vegetation volume formed by four Ficus plants.

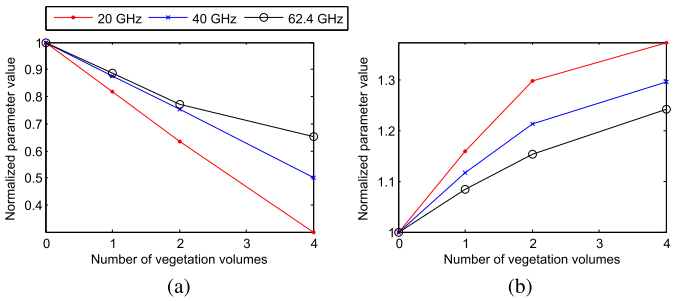

Fig. 10. Variation phase function parameters. (a) α. (b) β.

TABLE I

α AND β VALUES EXTRACTED FROM MEASURED VEGETATION BLOCKS AT 20, 40, AND 62.4 GHz

	20 GHz		40 GHz		62.4 GHz	
Plant	α	β	α	β	α	β
FS	0.996	31.3°	0.9977	30.5°	0.9977	29.8°
F1	0.89	33.5°	0.924	31.7°	0.92	29.8°
F2	0.84	35.7°	0.86	31.6°	0.87	33.1°
F3	0.74	38.6°	0.83	38.3°	0.85	33.3°
F4	0.79	37.4°	0.88	34.6°	0.89	32.9°
2 Trees	0.63	40.6°	0.75	37.0°	0.77	34.4°
4 Trees	0.30	43.0°	0.50	39.5°	0.65	37.0°

The averaged reradiation functions recorded at these three frequencies were then used to extract α and β parameters by fitting the phase function given by (3) to the measured data. The reradiation function and their respective fitted phase functions obtained for *Ficus* F1 and for the group of four *Ficus* plants are depicted in Fig. 9(a) and (b), respectively. The broadening of the reradiation function forward lobe and the increase of the backscattering level can be verified as the vegetation volume size increases from Fig. 9(a) and (b). This behavior confirms the expected α and β variations, which can be further verified analyzing the data obtained from the remaining measurements performed at 20, 40, and 62.4 GHz, depicted in Table I.

To establish the variation of the relationship from the phase function parameters, their values were normalized to the FS results. In the particular case of the measurements performed with the single *Ficus* plant, an average from these four measurements was used. The plots presented in Fig. 10(a) and (b) depict the graphical representation of the α and β variation, with the increase of the vegetation volume, respectively, observed at 20, 40, and 62.4 GHz. At 20 and 40 GHz, the α parameter variation follows approximately a straight line. In the remaining situations, the parameter variation is not exactly linear; nevertheless, the approximation with a straight line seems to yield to negligible errors. The proposed variation of the relationship relies on a linear interpolation between two extreme known parameter sets, for the FS scenario and the maximum number of vegetation volumes. Such straight lines, representing the phase function parameter variation, can be expressed through

$$\begin{cases} \alpha(N_V) = \left[\dfrac{\alpha(N_{V\min}) - \alpha(N_{V\max})}{N_{V\min} - N_{V\max}}\right] N_V + \alpha(N_{V0}) \\ \beta(N_V) = \left[\dfrac{\beta(N_{V\min}) - \beta(N_{V\max})}{N_{V\min} - N_{V\max}}\right] N_V + \beta(N_{V0}) \end{cases} \tag{21}$$

where N_V represents the number of vegetation specimens, $N_{V\min}$ is the minimum number of vegetation tree widths used in the measurements (in the current case, the minimum number is zero corresponding to FS), $N_{V\max}$ is the maximum number of vegetation volumes, whereas $\alpha(N_{V0})$ and $\beta(N_{V0})$ represent the values of α and β obtained from the FS measurement, respectively. The assumption of a linear variation for the phase function parameters eventually generates an amount of error in the prediction of the phase function; however, given that the cell splitting will be useful when modeling trees exhibiting large canopies, a relatively good accuracy was achieved by (21) while predicting α and β parameters, since the prediction errors are below 0.05 for α and 4° for the β parameters. Although this seems to be a reasonable error, the effects caused by the introduction of these scaling errors in the dRET model results should be further evaluated.

The proposed parameter scaling method was assessed in a single tree geometry. To this extent, the dRET input parameters were extracted for an in-leaf *White Oak* tree with a 12 m of canopy diameter, using the method described in Section IV, at 20 and 40 GHz. The tree under test was then modeled using two different dRET simulation geometries. In the first, the tree is modeled by a single dRET cell and characterized by the propagation parameters directly extracted from the measurements, while in the second, the tree was split into 16 (4×4) cells, characterized by the scaled α and β parameters. The propagation parameters extracted from the *White Oak* tree at 20 and 40 GHz are presented in Table II. The predicted side scattered signals are subsequently evaluated using the dRET model for the two potentially equivalent scenarios. The results of this comparative analysis are depicted in Fig. 11(a) and (b) using 20 and 40 GHz parameters, respectively. Results obtained at 20 GHz show an excess attenuation difference of 6.2 dB between both the scenarios, whereas the results at 40 GHz exhibit a difference of 0.55 dB. The accuracy differences found for both the scenarios might be considered relatively substantial. However, the scaling methodology was only developed for one volume to four volumes splitting.

TABLE II
SCALED AND UNSCALED PROPAGATION PARAMETERS FROM THE *White Oak* TREE AT 20 AND 40 GHz

	Parameters	k_e	k_s	α	β_{-3dB}
20 GHz	Unscaled ($\Delta s = 12m$)	0.38	0.28	0.36	10.7°
	Scaled ($\Delta s = 3m$)			0.95	3.95°
40 GHz	Unscaled ($\Delta s = 12m$)	0.35	0.25	0.62	20.0°
	Scaled ($\Delta s = 3m$)			0.89	8.75°

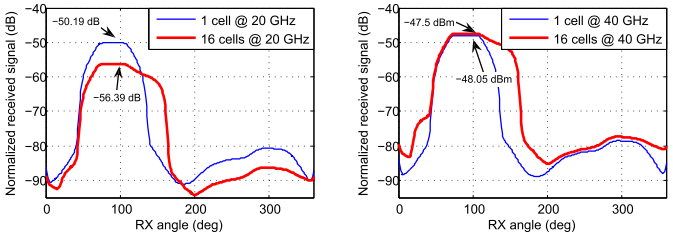

Fig. 11. Simulation results for the scattered signal of the *White Oak* tree at (a) 20 and (b) 40 GHz.

The highlighted examples represent a 16 to 1 reduction ratio, which pushes the parameter scaling method to its boundaries of validity. To this extent, further work should address a wider range of validation (and optimization) of the scaling method. Nevertheless, the relatively low differences between the results from both modeling scenarios suggests that the parameter scaling method is able to perform adequately for real-sized trees.

V. dRET TESTING USING IDEALIZED SCENARIOS

To test the proposed modified dRET model performance, two different forest scenarios were considered. Scenario 1 is formed by a single tree and is intended to study the shadowing effect, considering different TX locations, while Scenario 2 is formed by a screen of trees and an isolated block of vegetation. The aim of the latter is to show how the signal behind the screen of trees can be increased in the presence of the scattering effect from an isolated vegetation block.

A. Scenario 1: Single Vegetation Block

The detailed diagram of scenario 1 is presented in Fig. 12(a) and (b) considering two distinct TX locations. This scenario considers a 20 × 20 cell structure, each one with 1 m^2, composed by a 3 × 5 vegetation block, characterized by $\alpha = 0.95$, $\beta = 30°$, $k_e = 3$, and $k_s = 2.9$. The algorithm was simulated using an angular resolution of 1° while considering a 10 dBi RX antenna and an isotropic TX antenna. As depicted in Fig. 12, in both scenarios, the RX antenna orientation was kept constant at $\phi_{\text{RX}} = 0°$ and $\phi_{\text{RX}} \simeq 30°$ for TX positions 1 and 2, respectively.

Results from simulations performed with the dRET considering the two TX locations are depicted in Fig. 13. The coherent component attenuation causes the shadow effect due to the presence of the vegetation block in the radio path. The incoherent component is only formed inside the vegetation

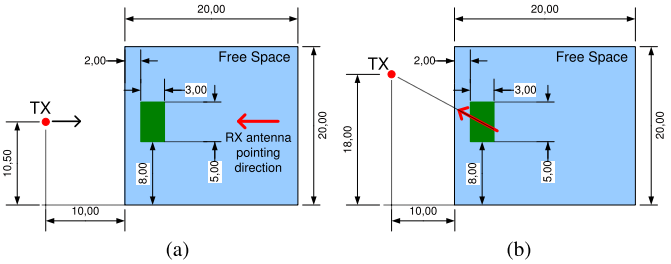

Fig. 12. dRET test scenario 1 for (a) TX position 1 and (b) TX position 2.

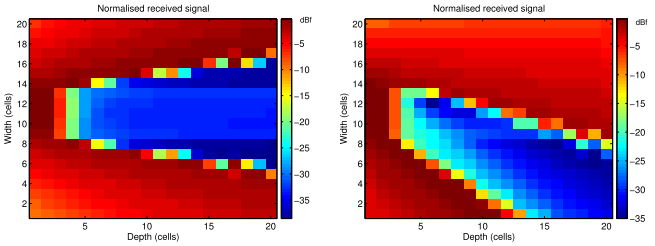

Fig. 13. $I_{\text{ri}} + I_d$ results for test scenario 1 considering a 10 dBi RX antenna for (a) TX position 1 and (b) TX position 2.

volumes. Hence, it causes the enhancement of the received signal behind the vegetation blocks, as suggested by the light blue shadows present behind the vegetation volumes.

The cells in scenario 1, which are not directly disturbed by the vegetation effect, exhibit an excess loss depending on the RX antenna location and consequently the relative TX–RX antenna alignment. This effect can be noted by the lighter red colors corresponding to lower received signal at those cells. In Fig. 13, the shadowing effect created by the vegetation block is also consistent when a point source illumination is considered, since the symmetrical shadow pattern (around the depth axes) obtained for scenario 1(a) is titled in scenario 1(b).

B. Scenario 2: Vegetation Screen + Isolated Vegetation Block

To test the dRET capability to predict the scattered signal generated from isolated vegetation blocks, a simulation geometry composed by a 4 m depth and 9 m wide vegetation screen, strategically positioned between the RX and TX antennas, and a 3 m ×2 m isolated vegetation block, as depicted in Fig. 14, was considered. This positioning aims to block the coherent signal component, allowing the incoherent signal scattered from the isolated vegetation block to be distinguished. Both blocks of vegetation included in this simulation scenario were modeled using the following parameters: $\alpha = 0.5$, $\beta = 10°$, $k_e = 0.5$, and $k_s = 0.4$.

Results obtained from the simulated vegetation structure are displayed in Fig. 15 for a cell size of 1 m and an angular resolution of 2°. Fig. 15(a) shows the coherent signal component at every cell of the computational volume considering an isotropic RX antenna. The plot shown in Fig. 15(b) represents the prediction of the directional spectrum of the received signal obtained with a 20 dBi and 20° of HPBW RX antenna, placed at the RX position.

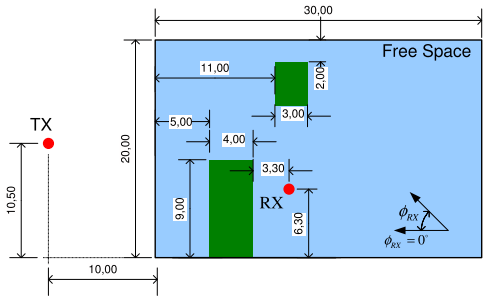

Fig. 14. Diagram of scenario 3 formed by a vegetation screen and an isolated vegetation block.

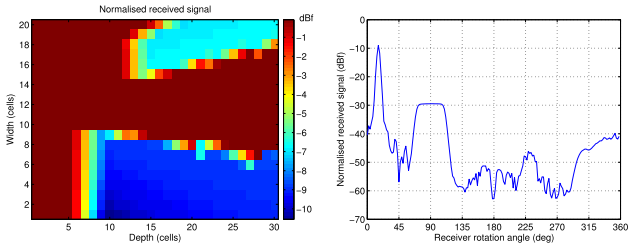

Fig. 15. Simulation results obtained for Scenario 2. (a) I_{ri} across the vegetation structure. (b) Directional spectra $I_{\text{ri}} + I_d$ at RX position.

The predicted signal incorporates both coherent and incoherent components. From the analysis of Fig. 15(b), it is evident that the maximum received signal level, corresponding to the coherent component, shows up at a ϕ_{RX} angle different from 0°. This is due to the assumption of a real point source instead of an idealized distant TX source. The coherent signal traveling through the vegetation screen is attenuated by approximately 10 dB, which is consistent with the attenuation shown in Fig. 15(a) and k_e value used throughout the simulation, i.e., $k_e = 0.5$. Around $\phi_{\text{RX}} = 90°$, the received signal directional profile exhibits a contribution due to the scattered signal from the isolated vegetation block. This shows that the modified dRET algorithm is capable of predicting the scattering, i.e., the incoherent signal, originated in an isolated vegetation structure located in the computational volume. The received signal decays considerably for $130° \leq \phi_{\text{RX}} \leq 300°$, because the RX antenna is pointing away from any vegetation. In this angular region, the received signal is mainly influenced by the rear of the RX antenna radiation pattern.

VI. Performance Analysis in Outdoor Inhomogeneous Tree Formation

The modified dRET model proved to be suitable to characterize the propagation in the presence of indoor tree formation scenarios [23], [24], with some degree of inhomogeneity, and to predict the directional spectra inside such vegetation structures at 20 and 62.4 GHz.

In this section, the proposed enhanced dRET model is used to predict the directional spectra for an outdoor inhomogeneous tree formation at two signal frequencies, i.e., 20 and 62.4 GHz. The performance of the proposed modified dRET model is assessed not only against site-specific directional spectra measurements but also against the current ITU-R recommendation for propagation in vegetation [6], which derives from the original RET formulation.

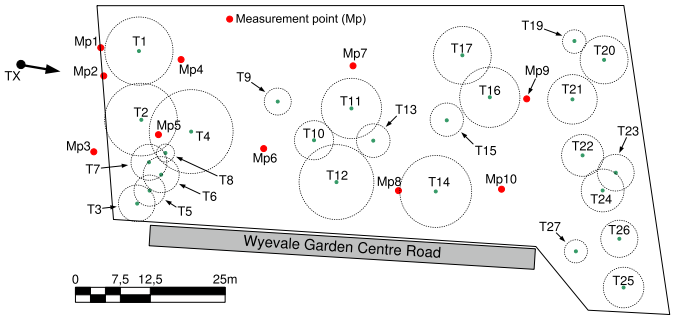

Fig. 16. Scaled map of Wyevale Garden Centre test site.

A. Methodology and Measurement Geometry

The measurement site is located in Cardiff, and a complete characterization of the test site geometry was achieved by measuring the tree locations and mean canopy diameters using a theodolite. The data gathered from these measurements were used to create the 2-D forest diagram depicted in Fig. 16. The tree positions, as well as the canopy diameters, are represented according to the scale shown in the diagram. The TX location employed throughout the directional spectrum measurements and its pointing direction are also shown in Fig. 16.

The test forest is then formed by 26 full size in-leaf trees, distributed by six different tree species. To individually identify each tree, they were labeled from T_1 to T_{27}. The characteristics of each tree, e.g., the species name and the approximate canopy diameter, are depicted in Table III. The *White Oak*, the *Prunus Sargentii*, and the *Prunus Avium* trees form large broad leaves, whereas the *Oleaster* and the *Pecan* show long needle shape ones. Finally, the *Betula Pendula* has the smallest leaves from all trees forming the Wyevale test site.

The directional spectra were then extracted with the RX placed at each one of the 10 measurement points (MPs), labeled from MP_1 to MP_{10} in Fig. 16. At each one of these MPs, the RX antenna was rotated around its vertical axes in a 360° angular range, with 1° increments, recording the received signal level arriving from various directions. Measurements at the two signal frequencies, i.e., 20 and 62.4 GHz, were performed independently, using the VV polarization configuration. In addition, both 20 and 62.4 GHz TXs employed relatively broad 10 dBi antennas so that a uniform air-to-vegetation interface illumination is ensured. At the RX end, high-gain antennas were employed, to provide a detailed and precise directional profile of the received signal. A 33 dBi antenna was used for 20 GHz measurements, whereas the 62.4 GHz measurement system employed a 36 dBi antenna.

To model the test forest using the dRET, a 38×18 (684) cell matrix was used, as depicted in Fig. 17. Each elementary cell was defined with 2.5 m^2, providing a good tradeoff between the computation effort and staircase error. In addition, this allowed the representation of the larger trees using 15–25 cells,

TABLE III

TREE TYPES PRESENT AT THE WYEVALE GARDEN CENTER TEST SITE AND SCALED PARAMETERS USED AT 20 AND 62.4 GHz

Tree Label	Species Name	Canopy (m)	SF	20 GHz		62.4 GHz	
				α	β	α	β
T_1		11.4	16.3	0.95	2.37°	0.92	2.14°
T_{15}		5.6	3.9	0.83	3.21°	0.74	2.26°
T_{16}	*White*	10.1	12.8	0.94	2.46°	0.90	2.15°
T_{20}	*Oak*	8.0	8.0	0.91	2.64°	0.86	2.18°
T_{23}		6.1	4.7	0.86	3.02°	0.78	2.23°
T_{24}		7.2	6.5	0.88	2.82°	0.82	2.20°
T_2		12.1	18.4	0.94	2.50°	0.93	2.47°
T_4	*Oleaster*	14.0	24.6	0.94	2.51°	0.92	2.48°
T_{12}		12.5	19.6	0.94	2.51°	0.92	2.48°
T_{14}		12.0	18.1	0.94	2.51°	0.92	2.48°
T_3		6.1	4.7	0.80	2.56°	0.77	3.67°
T_5		5.2	3.4	0.80	2.56°	0.77	3.67°
T_6	*Prunus*	6.0	4.5	0.80	2.56°	0.77	3.67°
T_7	*Sargentii*	6.0	4.5	0.80	2.56°	0.77	3.67°
T_8		3.0	1.1	0.80	2.56°	0.77	3.67°
T_{17}		9.6	11.6	0.91	2.97°	0.89	2.51°
T_9		4.5	2.5	0.62	4.50°	0.59	4.10°
T_{10}	*Betula*	6.5	5.3	0.81	3.25°	0.79	3.06°
T_{11}	*Pendula*	10.0	12.5	0.92	2.59°	0.89	2.51°
T_{13}		5.6	3.9	0.74	3.96°	0.77	3.80°
T_{19}		3.9	2.0	0.56	5.05°	0.52	4.54°
T_{21}		8.3	8.7	0.89	2.79°	0.86	2.67°
T_{22}	*Pecan*	7.0	6.2	0.85	3.08°	0.82	2.91°
T_{25}		6.8	5.8	0.84	3.12°	0.81	2.95°
T_{26}		6.2	4.8	0.81	3.32°	0.78	3.11°
T_{27}		3.9	1.9	0.53	5.27°	0.49	4.72°

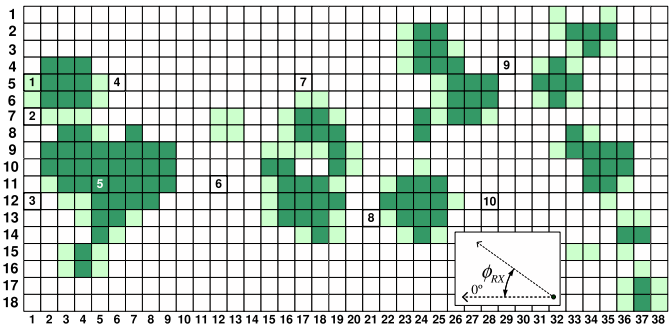

Fig. 17. dRET cells used for Wyevale test forest modeling.

which was just about the maximum scaling factor that could be accurately accommodated by the propagation parameter scaling method presented in Section IV.

Although it is possible to assign individual propagation parameters to the cells partially filled with vegetation, which consequently would enhance the model accuracy, this was not done in the current case study. Consequently, the propagation parameters were assigned on a frequency and tree basis, according to the methods depicted next, being identical and independent of the cell vegetation occupancy percentage. Cells with less than 50% of their area filled with vegetation were considered as air cells, shown in white color. The MPs were positioned at the nearest center from the corresponding cell. These positions, numbered from 1 to 10, are also shown in Fig. 17.

B. Parameter Extraction: Measurements and Results

To extract the relevant input propagation parameters required for the dRET modeling approach, the extraction method proposed in Section IV for outdoor scenarios was used. Under ideal circumstances, the parameter extraction procedure should be carried out in an isolated vegetation volume, as depicted in Fig. 6, hence avoiding any contamination of the measurements from other vegetation species. However, in the Wyevale test forest, it was impossible to find suitably isolated volumes of the relevant species present throughout the site. Consequently, the propagation parameters were extracted from trees located at the borders of the forest, thus limiting the amount of interference from the remaining vegetation. To further minimize any possible contamination, the TX antennas were positioned so that their main lobe illumination was limited to the vegetation block under measurement. The parameter extraction procedure was not performed for the *Pecan* trees, since this species was only found at the last vegetation row of the test forest and consequently would have a limited effect on the received signal level. Also, the analysis of the terrain surrounding these trees showed that it would be impossible to find sufficient foreground clearance to adequately perform the outlined measurements. These particular trees will be modeled using an average of the parameters extracted from the remaining trees.

The calculations of the k_e, k_s, α, and β propagation parameters were based on the received signal strength at M_2 and M_3 after being normalized to the received power at M_1. These measured normalized received signal levels are shown in Table IV, where $M_{3,1}$ is the difference between the maximum measured signals at M_3 and M_1, and $M_{2,1}$ stands for an average of M_2 signal obtained within a $\pm 15°$ angular range around the center of the tree, normalized to M_1. The analysis of the results from Table IV demonstrates that the sparser and smaller trees, e.g., T_1 and the $T_{3,5,6,7}$ tree group, tend to exhibit higher signal levels at M_3, when compared with M_2. This suggests that the received signal at M_3 is still due to the coherent signal component, whereas the signal at M_2 is due to the scattered or diffused component.

For trees where the coherent component has been excessively attenuated, the extinction coefficient extraction method may yield underestimated k_e values. An accurate extraction of this parameter should therefore be done using smaller volumes of vegetation, in order to ensure the presence of a significant coherent signal component at M_3. Due to the absence of smaller isolated vegetation volumes from the species of T_{11}, T_{12}, and T_{17}, where a better k_e estimation may be obtained, these trees were to be modeled using the available k_e estimations. The complete set of values for such k_e estimations is also presented in Table IV at the signal frequencies of 20 and 62.4 GHz.

The anticipated tendency for k_e to increase with frequency, due to the increasing absorption [6], [21], is only evident for the smallest vegetation group formed by the *Prunus Sargentii*. In the remaining cases, the k_e seems to stabilize, or even to decrease with frequency. This phenomena already reported by other researchers [25], [26] might be due to the fact that at high signal frequencies, the Fresnel ellipsoid clearance

TABLE IV
NORMALIZED RECEIVED SIGNAL LEVELS AT M_2 AND M_3 WITH RESPECT TO M_1, AND k_e, k_s, α, AND β PARAMETERS EXTRACTED FROM MEASUREMENT VEGETATION BLOCKS AT 20 AND 62.4 GHZ

Tree	20 GHz						62.4 GHz					
	$M_{3,1}$ (dB)	$M_{2,1}$ (dB)	k_e (Np/m)	k_s	α	β (deg)	$M_{3,1}$ (dB)	$M_{2,1}$ (dB)	k_e (Np/m)	k_s	α	β (deg)
T_1	-29.2	-51.7	0.37	0.28	0.35	6.41	-25.4	-47.3	0.30	0.13	0.08	2.8
$T_{3,5,6,7}$	-39.9	-60.2	0.98	0.24	0.13	4.20	-49.9	-58.8	1.26	1.02	0.07	15.5
T_{11}	-41.7	-52.2	0.75	-	0.05	8.20	-43.7	-46.7	0.81	-	-	12.1
T_{12}	-51.8	-52.7	0.68	-	-	9.54	-41.2	-56.0	0.50	0.10	0.15	14.8
T_{17}	-36.0	-47.9	0.45	-	0.13	11.7	-37.9	-49.9	0.49	0.37	0.04	11.1

decreases, and consequently, it is easier for the propagating signal to find free gaps through the vegetation structure. Other theory relates this odd behavior with the electrical and geometrical characteristics of the scatterers within the vegetation volume, assuming that the k_e stabilization with the increase of the signal frequency is related with a frequency resonance phenomenon.

Both α and β values obtained for each measured tree type present at the Wyevale test forest are presented in Table IV. The β values were optimized by fitting a Gaussian phase function to the directional signal profile obtained at measurement position M_3. By comparing the β values with the HPBW of the RX antennas used in the measurements and considering the relation $\beta = 0.6\mathrm{BW}_{-3\,\mathrm{dB}}$ [7], the broadening of the phase function forward lobe is evident. Although the RX antenna radiation pattern might cause a certain amount of distortion in the β measurement, the relatively low HPBW of the RX antennas employed should considerably limit this effect.

The α parameter optimization was based on the previously fitted β while considering the received signal level recorded at M_2. This method is not dependent on the RX antenna rotation and consequently was not affected by the RX antenna radiation pattern. However, a few trees exhibit a side scatter signal level similar to the signal level measured at M_3. Under these circumstances, the correct α parameter is somewhat difficult to be determined. The phase function α and β parameters shown in Table IV were obtained considering the complete trees. Consequently, they do not represent the 2.5 m size cells, used throughout the dRET vegetation modeling. To this extent, the dRET parameter scaling model was used to correct the α and β values extracted for the dRET vegetation cells. The final values for α and β used throughout the dRET simulations are depicted in Table III.

The determination of the scattering coefficient values k_s was performed as outlined in Section IV. This method is based on the previously calculated propagation parameters. Whenever it was impossible to find the phase function α parameter, an isotropic phase function was used in the optimization of k_s. Some of the k_s parameters were somewhat difficult to extract from the measured data, especially for the larger trees. This seems to be related to the above-mentioned difficulties arising from the high attenuation of the coherent signal component. The obtained k_s parameters are also shown in Table IV.

TABLE V
WYEVALE TEST FOREST RET INPUT PARAMETERS SETS

Pos.	Mean RET parameters	
	20 GHz	62.4 GHz
α	0.17	0.08
β	8.0°	11.3°
k_e	0.64	0.67
k_s	0.26	0.41
ω	0.41	0.61
γ_{R-3dB}	4.0°	2.8°

C. RET Simulation Parameters

This section provides a benchmark between the proposed enhanced dRET model and the original RET formulation, used in the current ITU-R 833-8 recommendation for propagation in vegetation [7], while predicting the directional spectra for an inhomogeneous outdoor tree forest scenario. The RET [8] theory is used to characterize through the component and consequently to predict the received signal level for various vegetation depths. This propagation model relies on a set of input parameters, including α and β used to manage the scattering function of the infinitesimal sized scatterers, the scattering and extinction coefficients, k_s and k_e, respectively, the albedo ω, which is the ratio between the scattered power, and the total power entering the random medium and the HPBW of the RX antenna ($\gamma_{R-3\,\mathrm{dB}}$). The RET model is exclusively derived for homogeneous vegetation media. To this extent and due to the inhomogeneity provided by the Wyevale forest, the RET input propagation parameters were characterized with the average values found for the various tree specimens. The RET input propagation parameters are depicted in Table V.

D. Results and Analysis

The proposed enhanced dRET model was used to predict the directional spectra at each one of the 10 RX positions, at 20 and 62.4 GHz. Simulation results were assessed not only against signal predictions using the original RET formulation but also against measurements performed for an outdoor inhomogeneous test forest, comprised by 26 trees of six different species.

Fig. 18(a) and (b) depicts the results obtained at measurement location MP_1, at 20 and 62.4 GHz. Although the

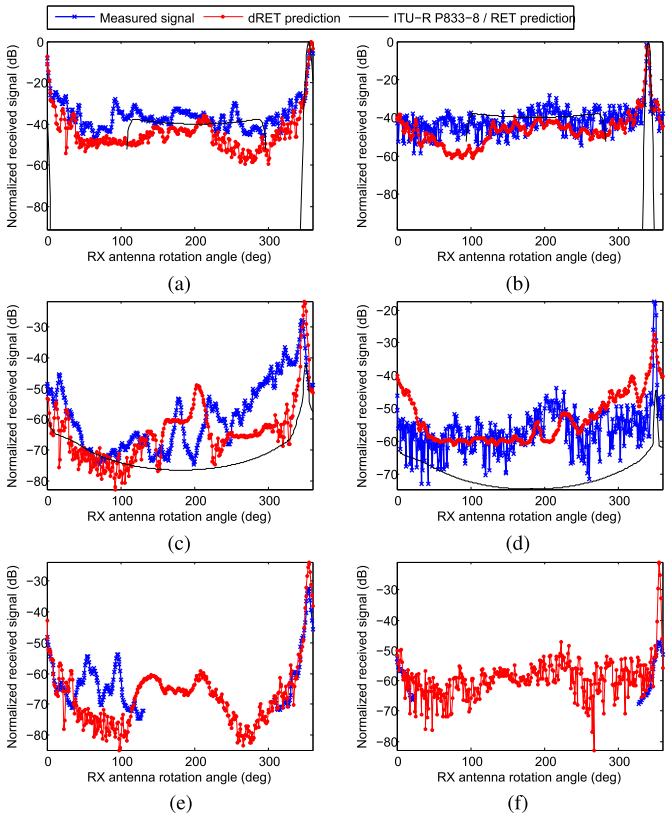

Fig. 18. Directional spectra results obtained at position: MP_1 at (a) 20 and (b) 62.4 GHz; MP_4 at (c) 20 and (d) 62.4 GHz; and MP_9 at (e) 20 and (f) 62.4 GHz.

directional spectra shape at MP_1 is mainly influenced by the RX antenna pattern, especially around the $\phi_{RX} \simeq 340°$ angular range, the TX and RX antennas are only facing each other in one particular antenna angle of the received signal directional spectrum. When the antennas are not pointing to each other, i.e., $\phi_{RX} \simeq 90°$ to $\phi_{RX} \simeq 270°$, an important part of the received signal is emanated from the backscattering of the forest. To this extent, the approximations of the estimation of the backscattering intensity might lead to the differences found between both measured and dRET results. In addition, effects such as the ground reflection and possible scattering in the remaining environment (which were not included in the model), may be responsible for the inaccuracies depicted in Fig. 18(a) and (b).

Results obtained at MP_4 are depicted in Fig. 18(c) and (d). This position is located behind tree T_1, and consequently, the received signal level is influenced by the estimated k_e parameter corresponding to this tree. In the angular region where the maximum signal was received, the absolute maximum error lies within 5 and 10 dB for 20 and 62.4 GHz, respectively.

These relatively low errors are caused by fluctuations in the insertion loss due to the different radial paths, which the propagating signal used to travel through tree T_1. However, the imprecise evaluation of the scattering characteristics of *Oleaster* trees T_2 and T_4, which was based on the results obtained for tree T_{12}, resulted in a relatively inaccurate estimation of the scattered signal in the $260° \leq \phi_{RX} \leq 330°$ angular range. To this extent, an individual tree characterization would undoubtedly lead to a better overall performance of the dRET model.

Fig. 18(e) and (f) depicts the results obtained at MP_9, which is located at the rear of the test forest. All predictions show an rms error consistently below 10 dB, which can be considered to be satisfactory. The principal contribution for the overall error in the predictions obtained at 20 GHz is present at the $40° \leq \phi_{RX} \leq 100°$ directional range. Within these angles, the received signal is determined by vegetation surrounding the test forest rather than any modeled vegetation volume. Consequently, it is impossible for the dRET to predict such signal variations based on the forest model used. Considering the scattering originated within the test forest only, the agreement between the predicted directional spectrum and the actual received signal, which lies above the RX noise floor, can be considered good. At 62.4 GHz, the received signal strength at position #9 was only measurable for a narrow angular range due to RX sensitivity limitations. The RET predictions obtained for measurement position MP_9 at 20 and 62.4 GHz severely underestimate the received signal level yielding to rms errors of about 150 dB; to this extent, data obtained using RET model was not included in Fig. 18(e) and (f).

A quantitative assessment on the performance of the modified dRET model while predicting the directional spectra for an outdoor inhomogeneous forest was performed for all the available measurement data. To this extent, the RMSE between the model prediction and the measured results was obtained for each of the 10 positions, at 20 and 62.4 GHz. However, at some measurement positions, the complete directional spectra were not possible to obtain due to RX sensitivity limitations. The complete summary on the RMSE analysis of dRET model predictions, as well as the number of available measurement samples per MP, are depicted in Table VI. The analysis of this table shows an expected trend for the RMSE to increase with the vegetation depth. Also, the positions influenced by the propagation characteristics of the *Oleaster* trees, i.e., MP_6, MP_8, and MP_{10}, seem to exhibit larger error values. These errors are believed to be due to the method used in the parameters extraction, which was based on a single tree measurement instead of averaging various trees.

As it would be expected, the majority of the dRET predictions were observed to be more accurate when compared with the RET model. This is mainly due to the inability of the RET in modeling a predominantly heterogeneous forest. However, at the air-to-vegetation interface, i.e., MP_1, MP_2, and MP_3, the received signal level is mainly influenced by both the RX antenna pattern and by the backscattering occurring in the first layer of trees. In these particular measurement positions, the RET model seems to provide a more reliable characterization of the backscattering phenomenon. However, this is due to the fact that RET considers a Gaussian antenna pattern in the simulations as opposed to a measured antenna pattern used in dRET (i.e., horn antenna), while in the former, there is only one Gaussian main lobe with no side- nor backradiation, i.e., a pencil sharp beam, and hence, no signal is being collected in the angular regions of 5°–108° and 296°–343° in MP_1. These correspond to the regions away

TABLE VI
RMS ERROR BETWEEN PREDICTED AND MEASURED VALUES AT WYEVALE TEST SITE

	RMSE (dB)				Number of points available	
	dRET model		RET model			
Pos #	20 GHz	62.4 GHz	20 GHz	62.4 GHz	20 GHz	62.4 GHz
MP_1	13.1	8.7	10.30	12.00	360	360
MP_2	10.3	9.2	10.40	13.20	360	360
MP_3	13.2	7.6	10.90	15.90	360	360
MP_4	10.1	7.9	14.40	17.40	360	360
MP_5	13.8	16.3	10.40	16.00	360	360
MP_6	17.1	15.3	45.60	51.70	360	193
MP_7	11.4	10.2	74.90	94.00	360	51
MP_8	22.1	20.3	94.40	98.70	185	116
MP_9	10.0	8.7	150.0	148.0	184	56
MP_{10}	6.6	-	146.0	-	26	0
Mean	12.8	11.6	56.72	51.88	-	-

from boresight and backscattering from semi-infinite air-to-vegetation interface, and therefore these angular ranges have not been considered for the computation of the rms error. As a consequence, in the latter, higher RMSE values were obtained, since the full angular range was considered.

Finally, an overall model performance with the mean RMSE from 9.0 to 12.8 dB was achieved by the dRET model. Although such errors are evaluated for the complete directional spectrum, these are similar to those reported in the literature obtained for simple attenuation versus depth measurements [6].

VII. CONCLUSION

A critical discussion of the original dRET modeling features, limitations, and drawbacks is presented in this paper. To overcome the original model drawbacks, new solutions were outlined yielding to an extended dRET formulation. The proposed modified dRET model includes the enhancement of the angular resolution, the simplification of the equations for both coherent and diffuse components, the integration of the RX antenna effect, the availability of a nonuniform interface illumination, and oblique incidence.

The dRET engine relies on four input propagation-dependent parameters. Considering the physical meaning of each parameter, an extraction method consisting of a limited number of measurements was also proposed. This method allows the optimization of the four dRET input parameters from isolated vegetation volumes, based on three relatively straightforward propagation measurements.

A thorough assessment on the enhanced dRET model was presented. The performance of the dRET modeling approach was assessed against directional spectra for an outdoor inhomogeneous tree formation at 20 and 62.4 GHz. As expected, the dRET greatly outperformed the RET formulation, which is derived for infinite homogeneous media. To this extent, the performance achieved by the modified dRET model was relatively good, since the overall RMSE achieved in a real outdoor environment was below 13 dB.

REFERENCES

[1] A. Ishimaru, *Wave Propagation and Scattering in Random Media*. Piscataway, NJ, USA: IEEE Press, 1997.

[2] F. Wang and K. Sarabandi, "An enhanced millimeter-wave foliage propagation model," *IEEE Trans. Antennas Propag.*, vol. 53, no. 7, pp. 2138–2145, Jul. 2005.

[3] K. L. Chee, S. A. Torrico, T. Kurner, "Radiowave propagation prediction in vegetated residential environments," *IEEE Trans. Veh. Technol.*, vol. 62, no. 2, pp. 486–499, Feb. 2013.

[4] S. A. Torrico and R. H. Lang, "Wave attenuation prediction through a volume of random located lossy-dielectric branches—3-D vector transport theory," in *Proc. 6th Eur. Conf. Antennas Propag. (EUCAP)*, Prague, Czech Republic, Mar. 2012, pp. 3342–3345.

[5] F. Wang, "Physics-based modeling of wave propagation for terrestrial and space communications," Ph.D. dissertation, Dept. Elect. Eng., Univ. Michigan, Ann Arbor, MI, USA, 2006.

[6] N. C. Rogers *et al.*, "A generic model of 1-60 GHz radio propagation trough vegetation—Final report," U.K. Radiocommun. Agency, Tech. Rep. QINETIQ/KI/COM/CR020196/1.0, May 2002.

[7] International Telecommunications Union (ITU), *Attenuation in Vegetation*, document Rec. ITU-R P.833-8, ITU-R, Geneva, Switzerland, 2013.

[8] R. Johnson and F. Schwering, "A transport theory of millimeter wave propagation in woods and forest," Forth Monmouth, Monmouth, NJ, USA, Tech. Rep. CECOM-TR-85-1, 1985.

[9] F. K. Schwering, E. J. Violette, and R. H. Espeland, "Millimeter-wave propagation in vegetation: Experiments and theory," *IEEE Trans. Geosci. Remote Sens.*, vol. GRS-26, no. 3, pp. 355–367, May 1988.

[10] M. O. Al-Nuaimi and R. B. L. Stephens, "Measurement and prediction model optimization for signal attenuation in vegetation media at centimeter wave frequencies," *IEE Proc.-Microw., Antennas Propag.*, vol. 145, pp. 201–206, Jun. 1998.

[11] G. Picard, T. L. Toan, S. Quegan, Y. Caraglio, and T. Castel, "Radiative transfer modeling of cross-polarized backscatter from a pine forest using the discrete ordinate and eigenvalue method," *IEEE Trans. Geosci. Remote Sens.*, vol. 42, no. 8, pp. 1720–1730, Aug. 2004.

[12] J. Richter, R. F. S. Caldeirinha, M. O. Al-Nuaimi, A. Seville, N. C. Rogers, and N. Savage, "A generic narrowband model for radiowave propagation through vegetation," in *Proc. IEEE 61st Veh. Technol. Conf. (VTC)*, vol. 1. May 2005, pp. 39–43.

[13] M. Mishchenko, L. Travis, and A. Lacis, *Multiple Scattering of Light by Particles: Radiative Transfer and Coherent Backscattering*. Cambridge, U.K.: Cambridge Univ. Press, 2006.

[14] M. Mishchenko *et al.*, "First-principles modeling of electromagnetic scattering by discrete and discretely heterogeneous random media," *Phys. Rep.*, vol. 632, pp. 1–75, May 2016.

[15] D. Didascalou, M. Younis, and W. Wiesbeck, "Millimeter-wave scattering and penetration in isolated vegetation structures," *IEEE Trans. Geosci. Remote Sens.*, vol. 38, no. 5, pp. 2106–2113, Sep. 2000.

[16] T. R. Fernandes, R. F. S. Caldeirinha, M. Al-Nuaimi, and J. Richter, "A discrete RET model for millimeter-wave propagation in isolated tree formations," *IEICE Trans. Commun.*, vol. E88-B, no. 6, pp. 2411–2418, Jun. 2006.

[17] F. T. Ulaby, T. H. Haddock, and Y. Kuga, "Measurement and modeling of millimeter-wave scattering from tree foliage," *Radio Sci.*, vol. 25, no. 3, pp. 193–203, May 1990.

[18] J. P. Gastellu-Etchegorry *et al.*, "DART: 3-D model of optical satellite images and radiation budget," in *Proc. IEEE Int. Geosci. Remote Sens. Symp. (IGARSS)*, vol. 5. Jul. 2003, pp. 3242–3244.

[19] Y.-Q. Jin and Z. Liang, "An approach of three-dimensional vector radiative transfer (3-D-VRT) equation for inhomogeneous scatter media," *IEEE Trans. Geosci. Remote Sens.*, vol. 42, no. 2, pp. 355–360, Feb. 2004.

[20] F. T. Ulaby, T. E. Van Deventer, J. R. East, T. F. Haddock, and M. E. Coluzzi, "Millimeter-wave bistatic scattering from ground and vegetation targets," *IEEE Trans. Geosci. Remote Sens.*, vol. 26, no. 3, pp. 229–243, May 1988.

[21] R. F. S. Caldeirinha, "Radio characterisation of single trees at micro- and millimetre wave frequencies," Ph.D. dissertation, School Electron., Univ. Glamorgan, Pontypridd, U.K., 2001.

[22] J. Richter, R. Caldeirinha, and M. Al-Nuaimi, "Phase function measurement for modelling radiowave attenuation and scatter in vegetation based on the theory of radiative energy transfer," in *Proc. IEEE Int. Symp. Pers., Indoor Mobile Radio Commun. (PIMRC)*, Sep. 2002, pp. 146–150.

[23] T. R. Fernandes, R. F. S. Caldeirinha, M. O. Al-Nuaimi, and J. Richter, "A discrete RET model for millimeter-wave propagation in isolated tree formations," in *Proc. IEICE Int. Symp. Antennas Propag. (ISAP)*, vol. 2. Sendai, Japan, Aug. 2004, pp. 817–820.
[24] T. R. Fernandes, R. F. S. Caldeirinha, M. O. Al-Nuaimi, and J. Richter, "A discrete model for radiowave scattering in vegetation screens at millimetric wave frequencies," in *Proc. IEEE 15th Int. Symp. Pers., Indoor Mobile Radio Commun. (PIMRC)*, vol. 1. Barcelona, Spain, Sep. 2004, pp. 1844–1849.
[25] A. Seville, "Vegetation attenuation: Modelling and measurements at millimetric frequencies," in *Proc. 10th Int. Conf. Antennas Propag.*, vol. 2. Apr. 1997, pp. 5–8.
[26] A. Seville and K. H. Craig, "Semi-empirical model for millimetre-wave vegetation attenuation rates," *Electron. Lett.*, vol. 31, no. 17, pp. 1507–1508, Aug. 1995.

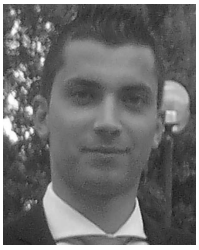

Nuno R. Leonor (S'15) was born in Leiria, Portugal, in 1988. He received the Licenciatura and M.Sc. degrees in electrical and electronics engineering and telecommunications from the School of Technology and Management, Polytechnic Institute of Leiria, Leiria, in 2010 and 2012, respectively. He is currently pursuing the Ph.D. degree with the University of Vigo, Vigo, Spain, with a focus on generic doubly selective 3-D vegetation model using point scatterers.

Rafael F. S. Caldeirinha (M'00–SM'15) was born in Leiria, Portugal, in 1974. He received the B.Eng. degree (Hons.) in electronic and communication engineering and the Ph.D. degree in radiowave propagation, with a focus on vegetation studies at frequencies from 1 to 62.4 GHz, from the University of South Wales, Pontypridd, U.K., in 1997 and 2001, respectively.

He has been the Head of the Antennas and Propagation Research Group, Instituto de Telecomunicações, Leiria, since 2010, and a Coordinator Professor in mobile communications and antennas and propagation with the School of Technology and Management, Polytechnic Institute of Leiria, Leiria, since 2001. He has authored or co-authored over 115 papers in conferences and international journals and four contributions to the International Telecommunications Union Recommendation (ITU-R) Study Group, which formed the basis of the ITU-R P.833-5 (2005) recommendation. His current research interests include the studies of radiowave propagation through vegetation media, including forest fire dynamics, radio channel sounding and modeling, and frequency selective surfaces, for applications at microwave and millimeter wave frequencies.

Dr. Caldeirinha is a member of the Editorial Board of the *International Journal of Communication Systems* (New York: Wiley) and a Fellow Member of the IET. He was the Program Chair of the WINSYS International Conference between 2006 and 2012. He has been the Chair of the IEEE Portugal Joint Chapter on Antennas and Propagation–Electron Devices–Microwave Theory and Techniques since 2016. He is an Associate Editor of the IEEE TRANSACTIONS ON ANTENNAS AND PROPAGATION and the *IET Microwaves, Antennas and Propagation*. He was an Appointed Officer for Awards and Recognitions of the IEEE Portugal Section in 2014. He has been a Regional Delegate of European Association for Antennas and Propagation for Andorra, Portugal, and Spain since 2017.

Telmo R. Fernandes (M'06–SM'16) was born in Coimbra, Portugal, in 1973. He received the Licenciatura degree in electrical engineering and telecommunications and electronics and the M.Sc. degree in electronic and telecommunication engineering from the University of Coimbra, Coimbra, in 1996 and 2000, respectively, and the Ph.D. degree in radio communication systems from the University of South Wales, Pontypridd, U.K., with a focus on radiowave propagation modeling through vegetation at millimeter-wave frequencies, in 2007. His M.Sc. thesis was entitled "Channel Assignment on Cellular Networks using Neural Networks and Genetic Algorithms."

In 1997, he joined the School of Technology and Management, Polytechnic Institute of Leiria, Leiria, Portugal, where he is currently an Adjunct Professor. From 2009 to 2011, he was the Head of the Electrical Engineering Department, and later in 2015, the Coordinator of the Electrical Engineering M.Sc. Course. He is currently a Researcher with the Antennas and Propagation Research Group, Instituto de Telecomunicações, Leiria. He has authored or co-authored over 75 scientific papers in international conferences and journals in the radiocommunications field. His current research interests include the studies of radiowave propagation through vegetation media at microwave and millimeter wave frequencies, frequency selective surfaces, energy harvesting, and electromagnetic compatibility.

Dr. Fernandes has been the Appointed Officer for the Conference Coordination of the IEEE Portugal Section since 2017.

Jürgen Richter received the Dipl.-Ing. degree from the Department of Electronics, Polytechnic Institute of Hanover, Hanover, Germany, in 1989, and the Ph.D. degree in radiowave propagation from the University of South Wales, Pontypridd, U.K., in 1998.

He is currently a Senior Lecturer with the Faculty of Engineering, University of South Wales, Pontypridd. He has been involved in studies on site shielding and vegetation at frequencies from 11 to 60 GHz.

Dr. Richter is a member of the IET.

Miqdad Al-Nuaimi received the B.Sc. degree (Hons.) in electronic and electrical engineering from the University of Birmingham, Birmingham, U.K., in 1967, and the Ph.D. degree in electronic and communication engineering from the University of Loughborough, Loughborough, U.K., with a focus on the radar detection theory, in 1972, and the D.Sc. degree with a focus on radiowave propagation and system design from the University of Glamorgan, Pontypridd, U.K., in 2006.

For over 30 years, he was with the communication industry and higher education, specializing in radiocommunication system and radiowave propagation. He is currently the Professor Emeritus with the University of South Wales, Pontypridd, U.K. He has authored or co-authored over 130 scientific papers.